STRUCTURAL SCIENCE
CRYSTAL ENGINEERING
MATERIALS

ISSN: 2052-5206
journals.iucr.org/b

Developing new SrI_2 and β-D-fructopyranose-based metal–organic frameworks with nonlinear optical properties

Domenica Marabello, Paola Antoniotti, Paola Benzi, Elena Cariati, Leonardo Lo Presti and Carlo Canepa

Acta Cryst. (2019). B**75**, 210–218

STRUCTURAL SCIENCE CRYSTAL ENGINEERING MATERIALS

ISSN 2052-5206

Developing new SrI_2 and β-D-fructopyranose-based metal–organic frameworks with nonlinear optical properties

Domenica Marabello,[a,b]* Paola Antoniotti,[a,b] Paola Benzi,[a,b] Elena Cariati,[c] Leonardo Lo Presti[c,d,e] and Carlo Canepa[a]

[a]Dipartimento di Chimica, University of Torino, via P. Giuria 7, Torino, 10042, Italy, [b]CrisDi-Interdepartmental Center for Crystallography, University of Torino, Torino, 10125, Italy, [c]Dipartimento di Chimica, Università degli Studi di Milano, Via C. Golgi 19, Milano, 20133, Italy, [d]Centre for Materials Crystallography, Århus University, Langelandsgade 140, Århus C, DK-8000, Denmark, and [e]Istituto di Scienze e Tecnologie Molecolari, Italian CNR, Via Golgi 19, Milano, I-20133, Italy. *Correspondence e-mail: domenica.marabello@unito.it

Received 6 November 2018
Accepted 4 February 2019

Edited by M. Du, Tianjin Normal University, People's Republic of China

Keywords: metal–organic frameworks; NLO properties; SHG efficiency; *ab initio* calculations; theragnosis; radiotherapy.

CCDC references: 1854903; 1854904; 1854905

Supporting information: this article has supporting information at journals.iucr.org/b

In the context of personalized medicine, there is a growing interest in materials bearing at the same time diagnostic and therapy functions. This article reports a cheap and easily reproducible procedure to obtain materials with a high potential for these applications. Three new strontium iodide–fructose-based metal–organic frameworks with formulae $[Sr(C_6H_{12}O_6)_2]I_2$, $[Sr_2(C_6H_{12}O_6)_3(H_2O)_3]I_4{\cdot}0.5H_2O$ and $[Sr(C_6H_{12}O_6)(H_2O)_3I]I$ differing in stoichiometry, symmetry and crystal packing, were obtained and characterized by X-ray diffraction. Bulk quantum simulations show that both the ions and the sugar are crucial in determining the predicted nonlinear response; also, the relative arrangement of various functional groups in the unit cell plays a role in the computed optical properties. Small fragments of the three compounds were selected for *in vacuo* calculations, proving that the reduced dimensions of the particles have a great influence on the nonlinear optical response. Despite the similar chemical composition of the three compounds, second harmonic generation measurements and *in crystal* and *in vacuo* theoretical calculations agree that one of the compounds is a much more efficient second harmonic emitter than the other two, and is thus a suitable candidate for bio-sensor applications.

1. Introduction

Nanomedicine is a relatively new branch of science, which is rapidly developing applications in diagnosis and treatment of many diseases and, in recent years, also in radiotherapy (Sheets & Wang, 2011). Combining in the same nanoparticles both light-based diagnostic and therapy functions has been attracting increasing interest in applied research for personalized medicine (Ryu *et al.*, 2014).

Among other diagnostic tools, of particular relevance are optical imaging techniques based on nonlinear optical (NLO) responses, such as the second harmonic generation (SHG) process (Boyd, 2003). Since SHG relies on light scattering rather than absorption, SHG-based nanoprobes neither bleach nor blink, and the signal does not saturate with increasing illumination intensity (Dempsey *et al.*, 2012; Pantazis *et al.*, 2010; McKinlay *et al.*, 2010; Campagnola & Loew, 2003). Thus, SHG-based imaging techniques provide the unique advantages of subcellular spatial resolution, high temporal resolution and sensitive detection at low concentration level (Liu *et al.*, 2017).

Lack of inversion symmetry in the crystal structure is mandatory to observe a solid-state SHG response. Sugars are

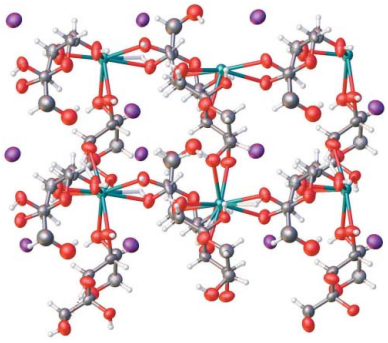

low-cost chiral ligands which are able to break the inversion symmetry in inorganic salts. We recently reported (Marabello *et al.*, 2015, 2017) a theoretical and experimental study on the NLO properties of metal–organic frameworks (MOFs) obtained from β-D-fructose and alkali-earth halogenides, MX_2 (M = Ca, Sr; X = Cl, Br). We showed that the coordination of fructose to a metal ion improves the second harmonic efficiency, probably by both inducing a lower symmetry and the dissociation of MX_2. Furthermore, the SHG intensity is mostly influenced by the anion, the first static hyperpolarizability (β) and second-order susceptibility ($\chi^{(2)}$) being higher for bromide compounds than for those with chloride. On the other hand, the cation seems not to play a significant role. Thus, in principle, iodide-containing MOFs should show even greater second harmonic efficiency. In this work, we verified this hypothesis with theoretical calculations and the positive results encouraged us to synthesize fructose-based Sr- and I-containing MOFs, which at the same time can also be useful for radiotherapy through substitution with ^{89}Sr and ^{131}I radioisotopes (Nightengale *et al.*, 1995; Yaneva *et al.*, 2005). We started from economical and biocompatible components, simple sugars and salts, and we combined them in new crystalline materials that can easily be converted into nanoparticles. We report the synthesis of three new strontium iodide-containing MOFs, of formulae $[Sr(C_6H_{12}O_6)_2]I_2$, (1), $[Sr_2(C_6H_{12}O_6)_3(H_2O)_3]I_4{\cdot}0.5H_2O$, (2), and $[Sr(C_6H_{12}O_6)(H_2O)_3I]I$, (3), where the same building blocks (Sr^{2+}, I^- and fructose) are organized in different stoichiometric ratios and different structural arrangements. The compounds were characterized by single-crystal X-ray diffraction. The first-order static hyperpolarizability and second-order susceptibility were estimated by *in vacuo* and *in crystal* theoretical calculations, and compared with experimental measurements of the SHG response of powdered samples.

2. Experimental

2.1. Synthesis of $[Sr(C_6H_{12}O_6)_2]I_2$, (1)

$SrI{\cdot}6H_2O$ and β-D-fructose, in the stoichiometric ratio 1:2, were dissolved in ethanol at 373 K. After a few minutes a faint precipitate was formed and the solvent was completely evaporated. Two drops of ethanol were added to the solid and the solid-solution mixture was left to equilibrate for a few hours, to obtain crystals suitable for X-ray diffraction (XRD) determination.

2.2. Synthesis of $[Sr_2(C_6H_{12}O_6)_3(H_2O)_3]I_4{\cdot}0.5H_2O$, (2)

$SrI{\cdot}6H_2O$ and β-D-fructose, in the stoichiometric ratio 2:1, were dissolved in acetonitrile at 373 K. After a few minutes a faint precipitate appeared which was decanted. The precipitate was dried in an oven at 303 K for a few hours and crystals suitable for XRD determination were formed on the walls of the vial.

2.3. Synthesis of $[Sr(C_6H_{12}O_6)(H_2O)_3I]I$, (3)

$SrI{\cdot}6H_2O$ and β-D-fructose were dissolved in acetonitrile at 353 K in the stoichiometric ratio 1:2. During the dissolution a faint precipitate was deposited at the bottom of the flask. The solution was discarded and the precipitate was dried in an oven at 303 K. After several hours many crystals suitable for XRD analysis were formed.

2.4. Single-crystal XRD

XRD data for compounds (1), (2) and (3) were collected at room temperature using an Oxford Diffraction Gemini R Ultra diffractometer. Data were collected with mirror-monochromatized Cu $K\alpha$ radiation (1.5418 Å) for compounds (1) and (2), and with graphite-monochromatized Mo $K\alpha$ radiation (0.71073 Å) for compound (3). The *CrysAlisPro* (Agilent Technologies, 2014) package was used for data collection and integration, *SHELXT* (Sheldrick, 2015) for resolution, *SHELXL* (Sheldrick, 2015) for refinement and *Olex2* (Dolomanov *et al.*, 2009) for graphics.

2.5. Computational methods

Bulk calculations. Periodic quantum simulations were carried out using the linear combination of Gaussian-type function (LCGTF) approach, implemented in the *CRYSTAL14* (Dovesi *et al.*, 2014) program. Both Hartree–Fock (HF) and density functional theory (DFT) PBE0 (Adamo & Barone, 1999) Hamiltonians were considered. C, H and O atoms were described by a 6-31G* split-valence basis set optimized for solid-state calculations (Gatti *et al.*, 1994), while Hay–Wadt pseudopotential libraries formerly employed for inorganic salts were associated with Sr^{2+} and I^- ions (Erba *et al.*, 2013; Doll & Stoll, 1998). For comparison purposes, a cheap, modified 3-21G all-electron split-valence basis (Binkley *et al.*, 1980; Dobbs & Hehre, 1987) set was also applied to all atoms. Hereafter, the two basis sets will be referred to as PS (pseudopotential) and AE (all-electron), respectively. All the calculations were based on the experimental structures retrieved from single-crystal XRD experiments. First, atomic coordinates were fully relaxed at fixed unit-cell parameters. Disorder was dealt with by repeating structure optimizations for each experimentally detected independent conformation or occupation in the asymmetric unit (see below). A supercell approach, where the disorder is directly included in the model to reproduce the experimental site-occupation factors, was not feasible due to impractical computational costs.[1] First-order polarizability and second-order susceptibilities were then estimated with the coupled-perturbed (CP) Hartree–Fock/Kohn–Sham method (Ferrero *et al.*, 2008*a*,*b*,*c*). Eventually, the same quantum simulations were also carried out on crystalline sucrose, which is usually employed as a standard reference for

[1] For example, we found that the CPU time *t*CPU for the PBE0/3-21G calculations is directly proportional to the number of atoms in the asymmetric units, n_A, according to an empirical law: *t*CPU (days) = 2.01 (9) n_A − 70 (5). This means that even a 2 × 2 × 1 supercell approach applied to compound (1), taking into account also the internal symmetry reduction, would roughly increase the computational time from 29 to 508 days of CPU time to achieve full convergence.

estimating the relative SHG response of sugars (Bourhill *et al.*, 1993), starting from the structure (Russo *et al.*, 2013) deposited in the Crystallographic Open Database (COD) (Grazulis *et al.*, 2009). Technical details of the computational procedure are available in the supporting information, Section S2, to ensure reproducibility of the discussed results.

In vacuo calculations. The calculations were performed with the *GAUSSIAN09* set of programs (Frisch *et al.*, 2009). All the structures in this work were optimized by gradient-based techniques (Schlegel & Daudel, 1981; Schlegel, 1982*a*,*b*; Schlegel *et al.*, 1984) with no symmetry constraints at the DFT B3LYP level of theory (Becke, 1988, 1993) in conjunction with the 6-31G(d) basis set for C, H, O atoms (Hehre *et al.*, 1986); for Sr and I the LANL2DZ basis was used (Wadt & Hay, 1985*a*,*b*,*c*). Any critical point was characterized as an energy minimum by calculating its analytical frequencies. Total dipole moment, polarizability and the first-order hyperpolarizability were calculated at the same level of theory. Molecular volumes were computed by averaging ten different volume calculations on the optimized geometries at the B3LYP level of theory with the *GAUSSIAN09* options scf = tight, volume = tight and iop(6/45 = 500, 6/46 = 1) (Parsons & Ninham, 2009).

2.6. SHG measurements

The SHG efficiency of powdered compounds was measured by the method of Kurtz and Perry (1968). Samples were ground in an agate mortar and heated in an oven at 323 K to avoid the absorption of humidity before being sealed into capillaries.

The 1064 nm wavelength of a Nd:YAG pulsed laser beam was directed on capillaries containing the samples. The scattered radiation was collected by an elliptical mirror, filtered to select only the second-order contribution, and recollected with a Hamamatsu R 5108 photomultiplier tube. The SHG efficiency was evaluated by taking as reference the SHG signal of sucrose.

3. Results and discussion

We recently analysed (Marabello *et al.*, 2017) the NLO properties of four isomorphic compounds of formula $[M(\text{fructose})_2(H_2O)_2]X_2{\cdot}H_2O$ (M = Ca, Sr and X = Cl, Br). As both the coefficients β_{tot} and $\chi^{(2)}$ are mainly] influenced by the anion (see Section 1), we performed *in vacuo* explorative calculations on the isomorphic fragment, reported in Fig. S1, pertaining to compounds with Sr^{2+}, Cl^- and Br^-. Substituting the anion with iodine, the β_{tot} and $\chi^{(2)}$ values obtained [21.5 × 10^{-30} cm^5 esu^{-1} (esu is electrostatic unit of charge) and 3.84 pm V^{-1}, respectively] are much higher. Thus, we also attempted to replace the halogen ion with iodide in the synthetic procedure: this led to compounds (1)–(3) with different structures compared with those containing chloride and bromide. This allowed us to study the NLO properties of compounds with different structural arrangements of the same building blocks.

3.1. Synthesis

Compounds (1), (2) and (3) were synthesized in two easy steps: (i) heating and evaporating water from the solutions with the reagents and (ii) recrystallization in a few drops of the same solvent. Thus, the compounds were synthesized with a simple, cheap and rapid method. This represents a good advantage for future preparations of the same materials with radioisotopes.

3.2. X-ray structure analysis

Compound (1) crystallizes in the monoclinic space group $P2_1$, a = 7.8592 (4), b = 12.9355 (5), c = 9.9504 (3) Å and β = 92.803 (4)°. The asymmetric unit contains one Sr^{2+} cation, two fructose molecules and two iodide anions (Fig. S2). Fig. 1 shows the coordination around the Sr cation: each Sr ion is surrounded by four fructose molecules, three of them bi-chelating and one three-chelating, behaving as bridges to the other Sr^{2+} cations. The C12H$_2$–O12H moiety is disordered over two positions with 59% and 41% refined site occupancies.

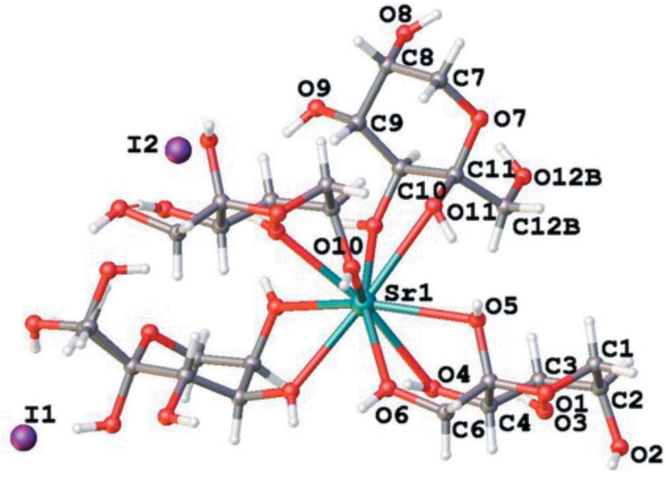

Figure 1
Coordination around the metal atom and atom labelling for (1).

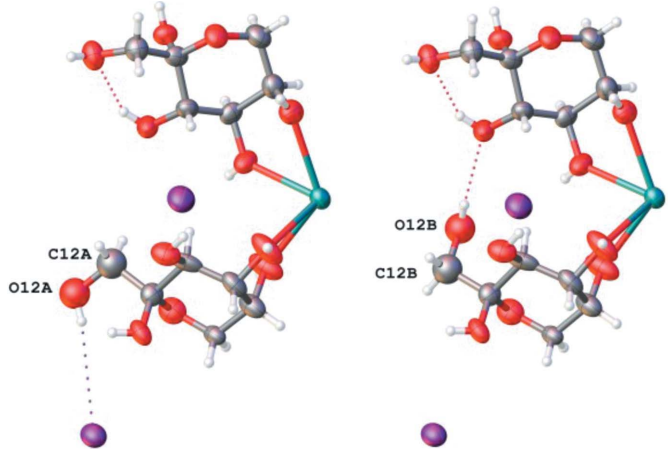

Figure 2
Conformational disorder of the C12H$_2$–O12H moiety of (1). *A* is 59% (on the left) and *B* is 41% (on the right) refined site occupancy.

The disorder can be defined as conformational, since a lateral –CH_2OH chain in one of the two symmetry-independent fructose units can assume two orientations, depending on whether the alcohol function forms a hydrogen-bonded contact with an I^- anion or with the pyranosidic oxygen of a translation–related sugar molecule (Fig. 2).

The Sr^{2+} cations and fructose in the crystal packing form extended wavy planes parallel to the *a* and *b* cell axes and stacked along the *c* axis (Fig. S3). Iodide atoms lie between planes and are connected to the fructose molecules through several hydrogen bonds (Table S3).

Compound (2) crystallizes in the orthorhombic space group $P2_12_12_1$, a = 12.3717 (2), b = 17.4352 (3), c = 17.6607 (3) Å. The asymmetric unit contains two Sr^{2+} ions, three fructose molecules, three water molecules, two of which are bonded to an Sr^{2+} cation and one is bonded to the other Sr^{2+}, four iodide ions and one free water molecule (Fig. S4). One Sr cation is surrounded by three sugar molecules, one bi-chelating and two three-chelating, while the second Sr^{2+} cation is surrounded by three bi-chelating sugar molecules and two water molecules (Fig. 3). Sr ions and fructose form infinite wavy planes parallel to the *a* and *b* cell axes and stacked along the *c* axis (Fig. S5). Iodide anions lie between planes and are connected to the fructose molecules through several hydrogen bonds (Table S3).

Compound (3) crystallizes in the orthorhombic space group $P2_12_12_1$, a = 9.1192 (3), b = 13.0908 (5), c = 13.5504 (8) Å. The asymmetric unit contains one Sr^{2+} ion, one fructose molecule, three water molecules bonded to the cation and two iodide ions (Fig. S6). One iodide ion is directly bonded to the Sr cation, at a distance of 3.724 (2) Å (Fig. 4), while the second iodide is connected to the water molecules through strong hydrogen bonds (Table S3). The $H_2O(3W)$ water molecule coordinated to Sr1 is disordered over two positions with 56% and 44% refined site occupancy (Fig. S6). The disorder can be defined as positional, since the two competing sites differ just with regard to the position of the single water molecule. The Sr^{2+} cations and sugar molecules alternate to form extended parallel threads along the *b* axis (Fig. S7), connected through hydrogen bonds through the iodide ions (Table S3).

While compounds (1) and (2) can be classified as bi-dimensional MOFs (2D-MOF), compound (3) is a 1D compound (1D-MOF). In any case, all compounds should be considered as non-conventional MOFs, since the spacer ligands are flexible neutral molecules and not anions. The anions are not involved in the MOF, instead being included in the crystal structure to fulfil electroneutrality.

Relevant bond distances for compounds (1)–(3) are reported in Table S2.

3.3. In-crystal computational results

The different crystal symmetry of compound (1) and sucrose (both $P2_1$) with respect to compounds (2) and (3) (both $P2_12_12_1$) has a significant influence on the allowed components of the first hyperpolarizability tensor, which must be invariant under any symmetry operation in the crystal system point group (Shen, 1984). It follows that in the orthorhombic 222 (D_2) group, only the d_{xyz} component is nonzero, and the equality $d_{xyz} = d_{xzy} = d_{zxy} = d_{zyx} = d_{yzx} = d_{yxz}$ holds true, meaning that just one symmetry-independent component is allowed. In this respect, it is indeed known (Chemla & Zyss, 1987) that monoclinic space groups are better than orthorhombic 222 ones at performing as good NLO solid-state chromophores. For these reasons, and because of the very high computational cost involved for compound (2), due to the greater dimensions of the unit cell, we preferred to focus on solid-state simulations of the more affordable compounds (1) and (3). Preliminary periodic PBE0/3-21G results for compound (2), however, were quantitatively very similar to those found for the symmetry-analogue compound (3). This is further confirmed by the

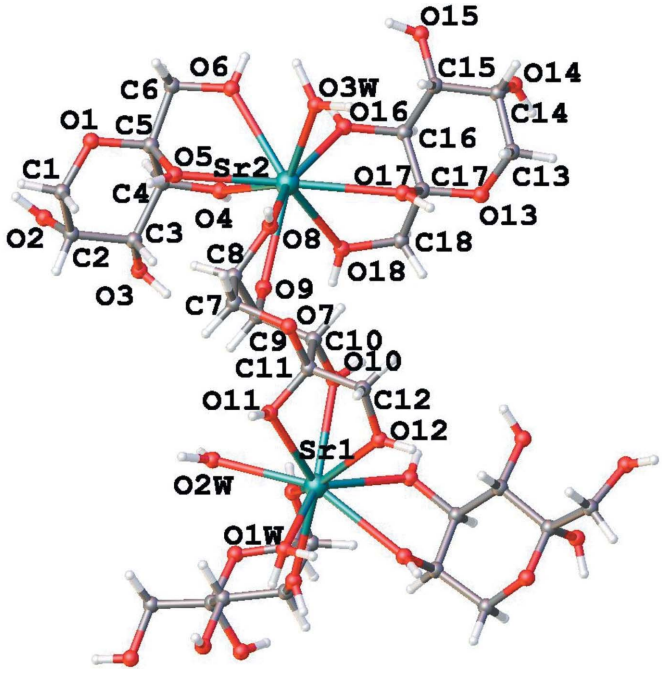

Figure 3
Coordination around the metal atoms and atom labelling for (2).

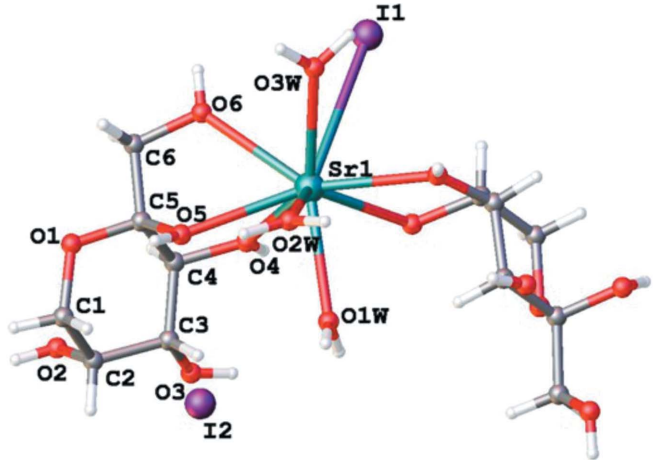

Figure 4
Coordination around the metal atoms and atom labelling for (3).

quantum simulations on isolated Sr–fructose complexes (see below).

From a geometric viewpoint, the optimized structures fully correspond to the experimental X-ray ones: the root-mean-square deviation (RMSD) on coordinates of C, O, Sr^{2+} and I^{-} atoms within the asymmetric unit backbone does not exceed 0.13 and 0.08 Å in compounds (1) and (3), respectively, at the PBE0/PS theory level; as expected, somewhat larger deviations affect hydrogen atoms. Fig. 5 shows the effect of different Hamiltonians and basis sets on the computed second-order optical properties of compounds (1) and (3). Full numerical entries, including the first-order polarizability estimates, are reported in the Tables S4 and S5.

The computed second-order optical properties of compound (3) and of sucrose appear to scarcely depend on Hamiltonians and basis sets, while compound (1) shows a remarkable increase from HF/AE to PBE0/PS level. A similar behaviour can also be inferred when the components of the first-order polarizability tensor are considered (Table S4). In general, both smaller basis sets and the neglect of Coulomb correlation effects imply a significant underestimation of the predicted tensor elements. The effect is particularly evident in fructose-containing compounds, where the square-averaged hyperpolarizability turns out to be 75–85% lower when a HF/3-21G method is employed rather than a more accurate PBE0/PS. On the other hand, in sucrose, where no metals are present, the maximum difference among the various computational approaches reduces to ≃30%. In any case, the nonlinear response is predicted to be up to an order of magnitude larger for compound (1) than for compound (3), while the latter should provide a nonlinear output comparable with that of sucrose. This result holds true independently of the computational level adopted (Fig. 5); thus, in the following we will focus the discussion on the highest-level PBE0/PS outcomes.

Table 1
First-order electric susceptibilities (dimensionless), diagonalized dielectric tensor elements (dimensionless) and second-order electric susceptibilities† at the PBE0/PS level of theory for compounds (1), (3) and sucrose.

For disordered structures, specific occupations of disordered sites (*A* or *B*, see text) are considered.

Substance	Compound (1)		Compound (3)		Sucrose
Space group	$P2_1$		$P2_12_12_1$		$P2_1$
Site‡	*A*	*B*	*A*	*B*	No disorder
Sof§	58.9	41.1	56.7	43.3	100.0
$\chi_{xx}^{(1)}$	1.2083	1.2183	1.1639	1.1386	1.1622
$\chi_{xz}^{(1)}$	−0.0067	−0.0211	0.0	0.0	−0.0435
$\chi_{yy}^{(1)}$	1.2714	1.2757	1.0521	1.0711	1.2136
$\chi_{zz}^{(1)}$	1.2339	1.2171	1.0021	0.9958	1.1750
ε_{11}	2.2066	2.2388	2.1639	2.1386	2.1247
ε_{22}	2.2714	2.2757	2.0521	2.0711	2.2136
ε_{33}	2.2355	2.1966	2.0021	1.9958	2.2125
$\chi_{xxy}^{(2)}$	1.0643	1.2055	0.0	0.0	0.1447
$\chi_{xyz}^{(2)}$	−0.2388	−0.1708	−0.1406	−0.1801	−0.0013
$\chi_{yyy}^{(2)}$	−0.7354	0.5362	0.0	0.0	0.2885
$\chi_{yzz}^{(2)}$	−0.4415	−0.5404	0.0	0.0	0.2048

† Atomic units. The same quantities can be expressed in other conventions through the usual conversion factors. Frequent alternative expressions of the second-order tensor components as β_{ijk} or d_{ijk} quantities [always in atomic units (a.u.)] are $\beta_{ijk} = (V\cdot\chi_{ijk})/2\pi$, V being the unit-cell volume in cubic bohr, and $d_{ijk} = \chi_{ijk}/2$. Conversion to the SI system in terms of reciprocal electric field units can be accomplished according to $d_{ijk}(\mathrm{SI}) = d_{ijk}(\mathrm{a.u.})/0.514220632$ pm V^{-1}. See also https://www.physics.nist.gov/cuu/Constants. ‡ For (1), *A* and *B* sites imply a different orientation of a terminal –CH_2OH chain, whereas for compound (3) they mark the different positions of a co-crystallized water molecule (see text). Sucrose bears no disorder. § Site-occupation factor (%).

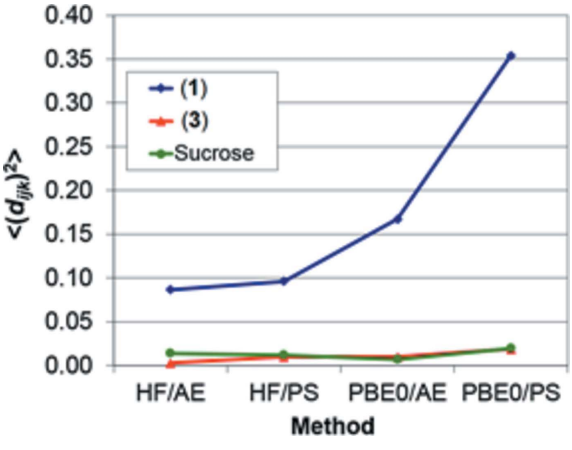

Figure 5
Averaged second electric susceptibility squared tensor elements (SI units) for compound (1), compound (3) and sucrose, as a function of the computational method. For disordered structures, just the most populated site is taken into account. PS: 6-31G* basis set, including Hay–Wadt pseudopotentials on Sr^{2+} and I^{-} ions; AE: all-electron 3-21G basis set.

The compounds (1) and (3) display conformational and positional disorder, respectively, resulting in different hydrogen-bonding networks (see above). Thus, both the possible site occupations (*A* and *B*) of disordered atoms were considered as starting points for geometry optimization. Table S6 summarizes the closest hydrogen-bonded contacts in the *A* (most populated) and *B* (least populated) arrangements (Figs. S8 and S9) after structure optimization. Our bulk theoretical model amplifies the mutually excluding coordination modes by exploiting Born−Von Karmàn periodic conditions, as if all the translation-related molecules in the crystal assumed either possible arrangement. We thus expect that the optical response of the experimental compound (1) and (3) crystals, where both the *A* and *B* coordination modes are present at the same time, will be close to the occupational-weighted average of the two predicted ones.

Table 1 compares the results of the second-order polarizability tensor elements for the majority (site *A*) and minority (site *B*) arrangements of disordered groups in compounds (1) and (3). First-order properties are barely affected, with maximum differences within the principal components not exceeding 1–2%. In contrast, differences as large as 10–20% affect the second-order properties. For compound (1), the component $\chi_{yyy}^{(2)}$ even reverses its sign when the least populated arrangement of the −CH_2OH chain is considered.

The present calculations demonstrate that the relative arrangement of various functional groups in the unit cell plays a not-negligible role in the computed optical properties, and in particular influences the NLO response.

SHG measurements and comparison with the bulk theoretical prediction. In non-phase-matchable compounds, when the average particle size, $\langle r\rangle$, is larger than the coherence length, l_c, the second-harmonic fields generated by different crystallites can be safely assumed to be uncorrelated with respect to each other (Shen, 1984). This means that the expected second harmonic intensity, $I^{2\omega}$, is proportional to $\langle d^2\rangle$, the angular average of the squared second-order polarizability tensor elements:

$$I^{2\omega} \propto \left\langle \left(d_{ijk}\right)^2 \right\rangle \frac{l_c^2}{2\langle r\rangle}. \quad (1)$$

Note that the d_{ijk} tensor elements are related to the χ_{ijk} ones shown in Table 1 through $d_{ijk} = \chi_{ijk} \times 0.972345$ (SI system, pm V^{-1}).

In phase-matchable materials, including sucrose (Russo *et al.*, 2013), some propagation directions exist in the crystal where l_c becomes very large, even larger than $\langle r\rangle$, and the second-order intensity should be expressed according to

$$I^{2\omega} \propto \frac{\pi^2}{4}\left(d_{ijk}^{PM}\right)^2 \frac{\pi \sin\theta_m}{\beta}. \quad (2)$$

Here θ_m is the angle between the phase-matching direction and the optic axis and $d_{ijk}{}^{PM}$ represents just the d_{ijk}, or the combination of d_{ijk}'s, for which phase matching occurs. The factor β is defined as

$$\beta = (\omega n_\omega^0 \sin\rho)/c, \quad (3)$$

where c is the speed of light, ω is the angular frequency of the fundamental (pumping) wave, $n_\omega{}^0$ the ordinary refractive index at the fundamental frequency and ρ the walk-off angle. According to equation (2), the second-order output does not depend on the particle size. However, it can be shown (Shen, 1984) that equation (2) holds true only when $\langle r\rangle >> \pi/\beta$, *i.e.* when the crystalline particles are large enough to allow the exploitation of the phase-matching conditions.

As for the present case, powders of both compounds (1) and (3) were ground in an agate mortar down to a particle size of the order of microns, so we can safely assume that both the conditions $\langle r\rangle >> l_c$ and $\langle r\rangle >> \pi/\beta$ are fulfilled (Russo *et al.*, 2013).[2] This also means that the second-harmonic efficiencies should not depend, on average, on the particle size, irrespective of the nature of the samples (phase-matchable or not). Therefore, square-averaged second-order polarizability tensor elements, $\langle d_{ijk}{}^2\rangle$, determine the relative second-order intensity ratio with respect to the sucrose. We computed $\langle d_{ijk}{}^2\rangle_{(1)}$, $\langle d_{ijk}{}^2\rangle_{(3)}$ and $\langle d_{ijk}{}^2\rangle_{sucrose}$ from periodic LCGTF solid-state simulations, by means of the weighted mean of the squared symmetry-independent tensor elements, $d_{ijk}{}^2$, in SI units. Symmetry multiplicities were used as weights for the monoclinic structure: 3 for d_{xxy} and d_{yyz}, 6 for d_{xyz} and 1 for d_{yyy}. It turns out that in both compounds (1) and (3), the least populated site B bears, on average, a slightly higher NLO response than the A one, as $\langle d_{ijk}{}^2\rangle_B > \langle d_{ijk}{}^2\rangle_A$ [0.41 versus 0.35 for (1) and 0.03 versus 0.02 for (3), in SI units]. To take into account the effect of the possible disorder distributed over sites A and B, each effective d_{ijk} element was calculated as the algebraic average of $d_{ijk}(A)$ and $d_{ijk}(B)$, weighted over the corresponding site-occupation factors. Table 2 reports the bulk $\langle d_{ijk}{}^2\rangle_X/\langle d_{ijk}{}^2\rangle_{sucrose}$ values and experimental $I^{2\omega}[X]/I^{2\omega}{}_{sucrose}$ relative efficiency for compounds (1) and (3).

Table 2
Ratio between the average second-order squared susceptibility tensor elements with respect to crystalline sucrose, as estimated through bulk calculations for compounds (1) and (3), compared with the SHG measurements.

	Compound (1)	Compound (3)
$\langle d_{ijk}{}^2\rangle/\langle d_{ijk}{}^2\rangle_{sucrose}$ (bulk)	19.2	1.2
$I^{2\omega}/I^{2\omega}{}_{sucrose}$ (measured)	10	1.5

From a qualitative viewpoint, theoretical calculations on the bulk agree with experimental measurements in predicting that compound (1) exhibits a second-order response larger than that of compound (3) by an order of magnitude. Interestingly, the same result holds true irrespective of the level of theory employed to derive the second-order susceptibility tensor elements (Tables S4–S8). However, for compound (1) the $\langle d_{ijk}{}^2\rangle_X/\langle d_{ijk}{}^2\rangle_{sucrose}$ ratio is significantly larger than the corresponding $I^{2\omega}/I^{2\omega}$(sucrose) one: this is due to the fact that the χ_{xxy} component is significantly greater than the χ_{xyz}, χ_{yyy} and χ_{zzy} ones, while just the opposite is true in sucrose (Table 1). It should be stressed, however, that quantum mechanical outcomes refer to ideal model systems at 0 K in the static field limit, and cannot take into account experimental effects, such as possible iso-orientations of crystallites and the dispersion behaviour of refractive indices at finite wavelengths.

Sublattice contributions to the SHG response. We also tried to understand to which chemical species (sugar, ions, water) should be ascribed the main contribution to the predicted second-order response. By definition, nonlinear effects are *not* pairwise additive, *i.e.* contributions to the total second-order susceptibility from different chemical species in the unit cell are not independent of each other. Accordingly, it is not possible to reconstruct any $\chi_{ijk}{}^{(2)}$ tensor element as a linear combination of independent terms associated with different substructures (Gavezzotti *et al.*, 2016; Colombo *et al.*, 2017).[3] However, if some tensor components of a given substructure are significantly higher than those of any other substructure, it

[2] In their seminal work on the SHG response of sugars, Bourhill *et al.* (1993) report that mean coherence lengths of their samples were all comparable and close to 20 mm.

[3] Analogously to the works of Gavezzotti *et al.* (2016) and Colombo *et al.* (2017), we define a substructure as a theoretical crystal structure which, keeping constant unit-cell edges and space-group symmetry of the parent crystal, is generated by any chemically sensible partition of the original asymmetric unit (ASU). For example, in (1) the ASU contains one fructose, one Sr^{2+} and two I^- ions. Suitable substructures are those generated either from the symmetry-independent sugar, without the ions, or from the symmetry-independent ions, without the sugar.

Table 3
Symmetry-independent second-order susceptibility tensor elements (atomic units) for organic and inorganic substructures in compounds (1) and (3).

The most populated disordered site was always considered. The same PBE0/PS level of theory and computational parameters as those employed for full structure calculations were exploited.

	Compound (1)		Compound (3)		
	Fructose	Ions	Fructose	Ions	Water
$\chi_{xxy}^{(2)}$	0.0260	−0.3376	0.0	0.0	0.0
$\chi_{xyz}^{(2)}$	0.0009	−0.2467	0.0158	0.1031	0.0094
$\chi_{yyy}^{(2)}$	0.1652	2.0123	0.0	0.0	0.0
$\chi_{yzz}^{(2)}$	−0.3139	−1.2015	0.0	0.0	0.0

is reasonable to assume that the contribution of that substructure to the second-order susceptibility of the whole crystal will be significant as well. We thus analysed both the organic (fructose) and the inorganic (water, ions) substructure contributions to nonlinear effects in compounds (1) and (3), by means of coupled-perturbed simulations at frozen unit-cell geometries and symmetries. Results are summarized in Table 3 and the same results as a function of the computational level are reported in Table S9.

At the PBE0/PS theory level considered here, the ions invariably provide the largest absolute tensor elements, even though fructose terms are not negligible. This likely implies that both the ions and the sugar are crucial in determining the predicted nonlinear response, the former being somewhat dominant. This suggests that a suitable strategy to enhance (or tune) the observed nonlinear response should mainly imply a change in the ionic framework of the crystal: if the symmetry remains favourable, a higher ionic polarizability should correspond to a more intense SHG output. This is also in agreement with previous findings by some of us (Marabello *et al.*, 2015, 2017).

3.4. *In vacuo* computational results and comparison with the SHG measurements

For *in vitro* biological applications, Sr–fructose MOFs have to be reduced to a particle size in the order of nanometres. The latter will be suitably functionalized on the surface in order to maximize the concentration inside or near the cancer cells. In this context, it is crucial to ascertain the SHG behaviour of small fragments of the compounds analysed, also considering the structural distortion that the surface forces can induce at the nanoscale level. To this end, small crystal fragments of the three compounds were selected (Figs. S10, S11 and S12) and the relevant geometries were recomputed by optimizing the atomic coordinates derived from the X-ray structures. The composition of the fragments does not reflect their stoichiometry, but an excess of sugar molecules was added at the boundary of the structure to attain full coordination of the metal. The fragment of compound (1) is composed of three strontium ions, eight fructose molecules and six iodide ions. The fragment of compound (2) is formed by three strontium ions, seven fructose molecules, six iodide ions and eight water molecules, five of which are bonded to Sr^{2+} cations, and three free water molecules. The fragment of compound (3) contains four strontium ions, six fructose molecules, eight iodide ions and 12 water molecules, all bonded to the strontium ions. Since sucrose is the reference compound usually used for SHG measurements, the same type of calculation as those performed on the fragments was carried out on a model of bulk sucrose composed of four sucrose units from the crystal structure in the Cambridge Structural Database [CCDC 835302] (Fig. S13). All geometries were re-optimized at the B3LYP level of theory to obtain the corresponding minima.

As expected, the optimized structural parameters show deviations from the corresponding X-ray data (Table S2): the maximum difference between the calculated and experimental average atomic distances ranges between 2% of the Sr—O averaged bond distance to 17% of the Sr···I averaged interatomic distance, probably due to the small size of the computed fragment, which involves a certain degree of asymmetry with respect to the crystal.

The total dipole moments μ and the mean polarizabilities $\langle\alpha\rangle$ in a Cartesian frame are defined as

$$\mu = \left(\mu_x^2 + \mu_y^2 + \mu_z^2\right)^{1/2}, \tag{4}$$

$$\langle\alpha\rangle = (1/3)\left(\alpha_{xx} + \alpha_{yy} + \alpha_{zz}\right). \tag{5}$$

The total intrinsic hyperpolarizability $\beta_{\rm tot}$ is defined as

$$\beta_{\rm tot} = \left(\beta_x^2 + \beta_y^2 + \beta_z^2\right)^{1/2}, \tag{6}$$

where $\beta_x = \beta_{xxx} + \beta_{xyy} + \beta_{xzz}$, $\beta_y = \beta_{yyy} + \beta_{yzz} + \beta_{yxx}$ and $\beta_z = \beta_{zzz} + \beta_{zxx} + \beta_{zyy}$ (Kanis *et al.*, 1994; Kyrill *et al.*, 2008).

The relationship between the macroscopic second-order susceptibility, the quantity that correlates to the second harmonic intensity, and the microscopic total hyperpolarizability is given by equation (7):

$$\chi^{(2)} = \beta_{\rm tot}/\varepsilon_0 V, \tag{7}$$

where V is the molecular volume.

In Table 4 the computed values of the dipole moment (μ), mean polarizability ($\langle\alpha\rangle$), first static hyperpolarizability ($\beta_{\rm tot}$) and second-order susceptibility ($\chi^{(2)}$) are reported for all compounds. The ratio between the second-order susceptibility of the compounds and that of sucrose is also reported, in order to be able to compare the computational results with the experimental second harmonic measurements.

Table 4 shows that the values of $\langle\alpha\rangle$ are similar for the three compounds, while the dipole moments are affected by the different cluster structures, as compound (3) shows a dipole moment smaller than the other compounds. The hyperpolarizability β and the static susceptibility $\chi^{(2)}$ values are also influenced by the cluster structure, compound (1) showing the highest values with respect to compounds (2) and (3). This trend is confirmed by comparing the $\chi^{(2)}/\chi^{(2)}_{\rm sucrose}$ ratios with the measured $I^{2\omega}/I^{2\omega}_{\rm sucrose}$ values. Interestingly, *in vacuo* results are qualitatively similar to the *in crystal* ones (compare Table 4 with Tables 1 and 2), even though the difference in the

Table 4
In vacuo computed dipole moments μ (Debye), mean polarizabilities $\langle\alpha\rangle$ (a.u.), first static hyperpolarizabilities β_{tot} (10^{-30} cm^5 esu^{-1}), second-order susceptibilities $\chi^{(2)}$ (pm V^{-1}), and second-order susceptibility ratios with respect to sucrose values for compounds (1)–(3).

	(1)	(2)	(3)
μ	22.466	22.952	12.196
$\langle\alpha\rangle$	862.008	835.740	840.989
β	27.0	18.0	14.7
$\chi^{(2)}$	4.23	2.86	2.25
$\chi^{(2)}/\chi^{(2)}{}_{\text{sucrose}}$	3.0	2.0	1.6
$I^{2\omega}/I^{2\omega}{}_{\text{sucrose}}$ (measured)	10	2.0	1.5

calculated $\chi^{(2)}/\chi^{(2)}{}_{\text{sucrose}}$ between compound (1) and compounds (2)–(3) (1.0 and 1.4, respectively) is lower with respect to the measured $I^{2\omega}/I^{2\omega}{}_{\text{sucrose}}$ (8.0 and 8.5, respectively). It must be clarified that, while the *in vacuo* calculations are carried out on small fragments of the structures where the crystallographic symmetries are not taken into account, the experimental measurements are carried out on the crystalline powder of µm dimensions, where the surface tension effects do not prevail on crystal packing. Considering the differences between the solid-state structures and those of the isolated fragments, as well as the different levels of theory employed for periodic simulations, different quantum methods provide, in our opinion, a remarkable conformity of views. Comparing the experimental and theoretical results of compounds (1) and (3), it can be observed that the experimental NLO response is midway between the *in crystal* and the *in vacuo* calculations. This behaviour can be explained considering the dimension of particles, µm scale for the experimental measurements, and of a few nanometres for the *in vacuo* calculations, and at the same time considering that the *in crystal* calculations do not take into account the finite size of the crystal and its defects.

4. Conclusions

In this work, we synthesized three new iodide-containing compounds, starting from economical and biocompatible components (fructose and SrI_2), and we analysed their NLO response both theoretically and experimentally. The three compounds, even if they are composed of the same building blocks, show a very different NLO response that is strictly related to the different arrangements in the crystal structure. In particular, both the *in vacuo* and *in crystal* theoretical calculations suggest that compound (1) is the more efficient second harmonic emitter and experimental measurements of the SHG output qualitatively agree with the theoretical picture. Furthermore, the relative arrangement of various functional groups in the same unit cell has a role in the computed optical properties and both the ions and the sugar are crucial in determining the predicted nonlinear response.

The comparison between the NLO response predicted from *in vacuo* and *in crystal* calculations and the experimental one suggested that the experimental behaviour of real crystalline compounds is midway between the ideal *in crystal* calculations and the low-symmetry *in vacuo* calculations. Our predictions conform to the usual general trend, *i.e.* the lower the symmetry, the higher the NLO response (Beverina *et al.*, 2011).

Thus, we can conclude that nanoparticles of the material considered in this work, in particular of compound (1) that show the highest NLO response, are very promising as contrast agents in diagnostic molecular imaging and can be considered as a therapeutic means in ^{89}Sr- and ^{131}I-radiomedicine.

5. Related literature

The following references are cited in the supporting information: Dovesi *et al.* (2014), Broyden (1965), Johnson (1988), Lacivita *et al.* (2012, 2016).

Funding information

Financial support from MIUR (Ministero dell'Istruzione, dell'Università e della Ricerca) and Fondazione CRT is acknowledged. The Italian Supercomputing Centre CINECA is warmly thanked for providing computing time through the CINECA/Unimi convention. Thanks are also due to CINECA and Regione Lombardia for funding this work through the LISA initiative (project MODEFRUC).

References

Adamo, C. & Barone, V. (1999). *J. Chem. Phys.* **110**, 6158–6170.
Agilent Technologies (2014). *CrysAlisPro*. Version 1.171.37.31 (release 14-01-2014 CrysAlis171. NET, compiled Jan 14 2014, 18:38:05). Agilent Technologies, Yarnton, England.
Becke, A. D. (1988). *Phys. Rev. A*, **38**, 3098–3100.
Becke, A. D. (1993). *J. Chem. Phys.* **98**, 5648–5652.
Beverina, L., Sanguineti, A., Battagliarin, G., Ruffo, R., Roberto, D., Righetto, S., Soave, R., Lo Presti, L., Ugo, R. & Pagani, G. A. (2011). *Chem. Commun.* **47**, 292–294.
Binkley, J. S., Pople, J. A. & Hehre, W. J. (1980). *J. Am. Chem. Soc.* **102**, 939–947.
Bourhill, G., Mansour, K., Perry, K. J., Khundkar, L., Sleva, E. T., Kern, R., Perry, J. W., Williams, I. D. & Kurtz, S. K. (1993). *Chem. Mater.* **5**, 802–808.
Boyd, R. W. (2003). *Nonlinear Optics*. San Diego, USA: Academic Press, an imprint of Elsevier Science.
Broyden, C. G. (1965). *Math. Comput.* **19**, 577–593.
Campagnola, P. J. & Loew, L. M. (2003). *Nat. Biotechnol.* **21**, 1356–1360.
Chemla, D. S. & Zyss, J. (1987). *Nonlinear Optical Properties of Organic Molecules and Crystals*, Vol. 1. Orlando, USA: Academic Press Inc.
Colombo, V., Lo Presti, L. & Gavezzotti, A. (2017). *CrystEngComm*, **19**, 2413–2423.
Dempsey, W. P., Fraser, S. E. & Pantazis, P. (2012). *Bioessays*, **34**, 351–360.
Dobbs, K. D. & Hehre, W. J. (1987). *J. Comput. Chem.* **8**, 880–893.
Doll, K. & Stoll, H. (1998). *Phys. Rev. B*, **57**, 4327–4331.
Dolomanov, O. V., Bourhis, L. J., Gildea, R. J., Howard, J. A. K. & Puschmann, H. (2009). *J. Appl. Cryst.* **42**, 339–341.
Dovesi, R., Orlando, R., Erba, A., Zicovich-Wilson, C. M., Civalleri, B., Casassa, S., Maschio, L., Ferrabone, M., De La Pierre, M., D'Arco, P., Noël, Y., Causà, M., Rérat, M. & Kirtman, B. (2014). *Int. J. Quantum Chem.* **114**, 1287–1317.

Dovesi, R., Saunders, V. R., Roetti, C., Orlando, R., Zicovich-Wilson, C. M., Pascale, F., Civalleri, B., Doll, K., Harrison, N. M., Bush, I. J., D'Arco, P., Llunell, M., Causà, M. & Noël, Y. (2014). *CRYSTAL14 User's Manual*. University of Torino, Torino, Italy.
Erba, A., El-Kelany, Kh. E., Ferrero, M., Baraille, I. & Rérat, M. (2013). *Phys. Rev. B*, **88**, 035102.
Ferrero, M., Rérat, M., Kirtman, B. & Dovesi, R. (2008*a*). *J. Chem. Phys.* **129**, 244110.
Ferrero, M., Rérat, M., Orlando, R. & Dovesi, R. (2008*b*). *J. Chem. Phys.* **128**, 014110.
Ferrero, M., Rérat, M., Orlando, R. & Dovesi, R. (2008*c*). *J. Comput. Chem.* **29**, 1450–1459.
Gatti, C., Saunders, V. R. & Roetti, C. (1994). *J. Chem. Phys.* **101**, 10686–10696.
Frisch, M. J., Trucks, G. W., Schlegel, H. B., Scuseria, G. E., Robb, M. A., Cheeseman, J. R., Scalmani, G., Barone, V., Mennucci, B., Petersson, G. A., Nakatsuji, H., Caricato, M., Hratchian, X., Li, H. P., Izmaylov, A. F., Bloino, J., Zheng, G., Sonnenberg, J. L., Hada, M., Ehara, M., Toyota, K., Fukuda, R., Hasegawa, J., Ishida, M., Nakajima, T., Honda, Y., Kitao, O., Nakai, H., Vreven, T., Montgomery, J. A., Peralta, J. E. Jr, Ogliaro, F., Bearpark, M., Heyd, J. J., Brothers, E., Kudin, K. N., Staroverov, V. N., Kobayashi, R., Normand, J., Raghavachari, K., Rendell, A., Burant, J. C., Iyengar, S. S., Tomasi, J., Cossi, M., Rega, N., Millam, J. M., Klene, M., Knox, J. E., Cross, J. B., Bakken, V., Adamo, C., Jaramillo, J., Gomperts, R., Stratmann, R. E., Yazyev, O., Austin, A. J., Cammi, R., Pomelli, C., Ochterski, J. W., Martin, R. L., Morokuma, K., Zakrzewski, V. G., Voth, G. A., Salvador, P., Dannenberg, J. J., Dapprich, S., Daniels, A. D., Farkas, Ö., Foresman, J. B., Ortiz, J. V., Cioslowski, J. & Fox, D. J. (2009). *GAUSSIAN09*, Revision A02. Gaussian, Inc., Wallingford, CT, USA.
Gavezzotti, A., Colombo, V. & Lo Presti, L. (2016). *Cryst. Growth Des.* **16**, 6095–6104.
Grazulis, S., Chateigner, D., Downs, R. T., Yokochi, A. F. T., Quirós, M., Lutterotti, L., Manakova, E., Butkus, J., Moeck, P. & Le Bail, A. (2009). *J. Appl. Cryst.* **42**, 726–729.
Hehre, W. J., Radom, L., Schleyer, P. von R. & Pople, J. A. (1986). *Ab Initio Molecular Orbital Theory*. New York: Wiley.
Johnson, D. D. (1988). *Phys. Rev. B*, **38**, 12807–12813.
Kanis, D. R., Ratner, M. A. & Marks, T. J. (1994). *Chem. Rev.* **94**, 195–242.
Kurtz, S. K. & Perry, T. T. (1968). *J. Appl. Phys.* **39**, 3798–3813.
Kyrill, Y., Suponitsky, K. Y., Tafur, S. & Masunov, A. E. J. (2008). *Chem. Phys.* **129**, 044109.
Lacivita, V., Rérat, M., Orlando, R., Dovesi, R. & D'Arco, P. (2016). *Theor. Chem. Acc.* **135**, 81.
Lacivita, V., Rérat, M., Orlando, R., Ferrero, M. & Dovesi, R. J. (2012). *Chem. Phys.* **136**, 114101.
Liu, T.-M., Conde, J., Lipiński, T., Bednarkiewicz, A. & Huang, C.-C. (2017). *Prog. Mater. Sci.* **88**, 89–135.
Marabello, D., Antoniotti, P., Benzi, P., Canepa, C., Diana, E., Operti, L., Mortati, L. & Sassi, M. P. (2015). *J. Mater. Sci.* **50**, 4330–4341.
Marabello, D., Antoniotti, P., Benzi, P., Canepa, C., Mortati, L. & Sassi, M. P. (2017). *Acta Cryst.* B**73**, 737–743.
McKinlay, A. C., Morris, R. E., Horcajada, P., Férey, G., Gref, R., Couvreur, P. & Serre, C. (2010). *Angew. Chem. Int. Ed.* **49**, 6260–6266.
Nightengale, B., Brune, M., Blizzard, S. P., Ashley-Johnson, M. & Slan, S. (1995). *Am. J. Health Syst. Pharm.* **52**, 2189–2195.
Pantazis, P., Maloney, J., Wu, D. & Fraser, S. E. (2010). *Proc. Natl Acad. Sci.* **107**, 14535–14540.
Parsons, D. F. & Ninham, B. W. (2009). *J. Phys. Chem. A*, **113**, 1141–1150.
Russo, L., Gražulis, S. & Bagdziunas, G. (2013). Personal communication to COD. This structure is available in the Crystallography Open Database (COD, http://www.crystallography.net/) with number 3500015.
Ryu, J. H., Lee, S., Son, S., Kim, S. H., Leary, J. F., Choi, K. & Kwon, I. C. (2014). *J. Controlled Release*, **190**, 477–484.
Schlegel, H. B. (1982*a*). *J. Chem. Phys.* **77**, 3676–3681.
Schlegel, H. B. (1982*b*). *J. Comput. Chem.* **3**, 214–218.
Schlegel, H. B., Binkley, J. S. & Pople, J. A. (1984). *J. Chem. Phys.* **80**, 1976–1981.
Schlegel, H. B. & Daudel, C. (1981). *Computational Theoretical Organic Chemistry*. Reidel Publ. Co.
Sheets, N. C. & Wang, A. (2011). *Radioisotopes – Applications in Bio-Medical Science*, edited by P. N. Singh, pp. 47–66. Rijeka: InTech.
Sheldrick, G. M. (2015). *Acta Cryst.* C**71**, 3–8.
Shen, Y. R. (1984). *The Principles of Nonlinear Optics*. *Wiley Series in Pure and Applied Optics*. New York, USA: Wiley.
Wadt, W. R. & Hay, P. J. (1985*a*). *J. Chem. Phys.* **82**, 270–283.
Wadt, W. R. & Hay, P. J. (1985*b*). *J. Chem. Phys.* **82**, 284–298.
Wadt, W. R. & Hay, P. J. (1985*c*). *J. Chem. Phys.* **82**, 299–310.
Yaneva, M. P., Semerdjieva, M., Radev, L. R., Ivanova, E. K., Geiman, M., Vlaikova, M. I. & Mihova, L. S. (2005). *Folia Med. (Plovdiv)*, **47**, 63–69.